SuPreMeChiF – a New Approach to Detect Subtle Changes in Continuous Monitoring Data, with a case study of COVID-19 impact in Singapore through seismic and infrasound recordings

Y. Luo[1,2], B. Taisne[1,2], K. H. Lythgoe[1] and C.T. Tan[3]

[1] Earth Observatory of Singapore, Nanyang Technological University, Singapore.

[2] Asian School of the Environment, Nanyang Technological University, Singapore.

[3] Science Centre Board, Singapore.

Corresponding author: Yizhou Luo (yzluo@ntu.edu.sg)

Key Points:

- A new method is introduced that combines statistics and continuous spectral analysis to quantitatively detect subtle changes in a system.
- Results on Singapore seismic and infrasound during COVID-19 period agrees with mobility change timeline and reveals spectral details of the changes.
- The method has potential for real-time volcano monitoring in which subtle spectral content change could imply precursory activities.

Abstract

The lack of precursory signals at some volcanic eruptions could be due to the analysis performed which failed to capture subtle changes. We have developed a new technique, "Subtle Precursor Measurement of Change in Frequency (SuPreMeChiF)", which calculates the cumulative distribution difference (Kolmogorov-Smirnov test) between monitoring features in given reference and sample windows, to detect and quantify subtle changes in continuous data that may be overlooked by usual analysis. It is tested on seismic and infrasound recordings to analyse changes associated with the COVID-19 period, a known global perturbation. The results show high coherence with mobility, reveal details of changes that were not indicated in conventional spectral analysis, and demonstrate the potential to retrieve the source physical processes. This quantitative approach provides insight for future application in automated detections during real-time volcano monitoring.

Plain Language Summary

We introduce a new technique, "Subtle Precursor Measurement of Change in Frequency (SuPreMeChiF)", that detects subtle changes in a natural system by combining statistics and monitoring data analysis. Our method compares feature distributions in given reference and sample timeframe, during which subtle changes that may be overlooked by usual analysis can now be detected and quantified. We demonstrate our method using seismic and infrasound recordings in Singapore to analyse changes associated with the COVID-19 period, a known global perturbation. Results show high coherence with mobility trend, with clear detections of key events including the start of lockdown. The results also reveal details that were not indicated in conventional analysis, such as the frequency range where changes occurred. This demonstrates the potential to retrieve source mechanism information since frequency ranges can be indicative of physical processes. In this case study, changes in mobility were reflected in changes in background noise level recorded by local instrument – a situation analogous to volcano monitoring scenario, where disturbance in the volcanic system is reflected in changes in geophysical properties recorded by a monitoring network. Our next step includes applying SuPreMeChiF on known volcanic activities and considering future applications in automated detections during real-time monitoring.

1 Introduction

Volcanic eruptions can severely impact nearby communities (Janda et al., 1996) and have a composite, long-range impact on distant populations (Gudmundsson et al., 2012; Hansen et al., 1992). To mitigate the impact from volcanic eruptions, it is crucial to continuously monitor volcanic systems and identify/interpret abnormal behaviours which lead to disruptive volcanic activity. Continuous monitoring is achieved by installing permanent instruments on volcanoes that record changes in ground vibration, deformation, degassing and others (Sparks, 2003).

Some volcanic eruptions display clear precursor signals, while others have had few or no recognised indicators of an imminent eruption (Barberi et al., 1992; Maeda et al., 2015b; Smittarello et al., 2022). Un-forecasted volcanic eruptions are often referred to as "blue-sky" eruptions (Doherty, 2009; Jolly et al., 2010). However, for a volcano to erupt, there must be destabilisation of the system, either by energy input from the depth, in the form of gas (Germanovich & Lowell, 1995; Jolly et al., 2018), heat or magma (Aki & Koyanagi, 1981), or a destabilisation of the shallow part of the system from external forcing (Matthews et al., 2002; Neuberg, 2000; Seropian et al., 2021). The associated mechanism leading to the eruption is unlikely to happen without any physical or chemical perturbation. Therefore, regardless of timescale, any volcanic activity should be preceded by a certain level of precursory signal. The concept of "blue-sky" eruptions could be seen as a "cloudy-sky" situation, in which precursory signals did exist but were missed during real-time analysis of monitoring data either due to the method used, the type of monitoring instruments or their location.

Most commonly used volcano monitoring techniques are based on seismic data. One widely-used example is Real-time Seismic Amplitude Measurement (RSAM), which measures average seismic amplitude in continuous waveform data, and triggers alerts when the amplitude exceeds a set threshold (Endo & Murray, 1991). However, subtle changes in volcanic systems may be frequency dependent and/or may not be reflected in noticeable seismic amplitude differences. In addition, the effectiveness of the critical threshold is limited by the signal to noise ratio (SNR) of the data. Another popular tool for volcano monitoring uses seismic noise to detect changes in seismic velocity (Brenguier et al., 2008; Lecocq et al., 2014). However, the detection capability may similarly be restricted in noisy environments. Stacking is usually involved over long-time scales to increase the SNR, which may result in missing short-term events.

More "hidden" features of continuous monitoring data, such as its frequency content, may be better indicators of subtle changes in the system. Changes in the spectral content of continuous seismic data is analysed in the Self-Organising Maps (SOM) algorithm, which uses machine learning to cluster data based on similar frequency content (Klose, 2006). SOM has proved effective in detecting tremor before eruptions at Mt. Etna (Langer et al., 2009) and Ruapehu volcano (Carniel et al., 2013). However, the limited number of pre-defined clusters restricts the method's sensitivity and therefore it may not be as effective in detecting subtle changes. Furthermore, SOM processes the whole time-series at once and does not take into account cyclic patterns (e.g., diurnal changes) which could complicate the identification of precursory signals.

In this paper, we develop a new technique to quantify subtle changes in a system that may be overlooked by conventional analysis. Our method, "Subtle Precursory Measurement of Change in Frequency (SuPreMeChiF)", is a universal and quantitative analysis that combines a statistical Kolmogorov-Smirnov (K-S) test with monitoring data analysis, to detect subtle signs of perturbations in continuous monitoring data.

Kolmogorov-Smirnov (K-S) tests have been successfully applied to monitor changes in continuous data across a wide range of fields. Recent studies in engineering have revealed its potential in condition monitoring of machinery. For example, early-stage machinery failure can be detected by comparing the probability distribution of sample vibration signals to that of template signatures of known conditions (Wang & Makis, 2009). Several studies have used K-S tests in fault diagnosis and performance degradation assessment for rolling bearings (Cong et al., 2011; Kar & Mohanty, 2004). This situation is analogous to our case, in which we look for any abnormality or precursory signals before a failure, or internal/external perturbations in the natural system. For a natural environment setting, Mulargia et al. (1987) has first implemented the K-S test on accumulative eruption count to identify change points that divide regimes during eruptive history on Etna. Since then, K-S tests have been used to analyse cumulative eruption volume (Burt et al., 1994) and forecast assessment (Bebbington, 2013). K-S analysis has not yet been adopted for real-time analysis on continuous monitoring data.

We first introduce the SuPreMeChiF method and apply it to synthetic data. We then illustrate its capability at detecting subtle changes in continuous data by applying it to local

seismic and infrasound waveforms. The coronavirus pandemic that struck in 2020 caused a global quiescence in high-frequency seismic noise due to lockdown measures (Lecocq et al., 2020). Here we use the Singapore COVID-19 period as a test case for our SuPreMeChiF method, in which the timeline of changes due to anthropogenic activity is known and well-constrained. Our analysis includes infrasound monitoring data to further illustrate the method's potential, since changes in infrasound data were smaller and less distinct than in seismic data. Lastly, we discuss the results and potential for real-time volcano monitoring.

2 SuPreMeChiF methodology

2.1 Data Pre-processing

The raw waveform is first transferred into the frequency domain using the continuous wavelet transform (CWT). The CWT has advantage over the Discrete Fourier Transform in providing better time-frequency resolution (Chakraborty & Okaya, 1995; Lapins et al., 2020). The resulting frequency information is presented in power spectral density (PSD) with the frequency range in a logarithmic scale. We use a Morlet wavelet of window length 1800 seconds, which balances the trade-off between time and frequency resolution, as well as computational cost. To minimise potential edge effects, we extract only the middle one-third (600s) of each CWT window, with the window moving along the full timeline with two-thirds overlap. The resulting PSD is then decimated from the original sampling rate (100 Hz) to one value per second (1 Hz) by calculating the average in a 1 second window. The resulting matrix comprises the power spectral density categorised in log-scale frequency bins at each second along the timeline.

2.2 Kolmogorov-Smirnov Test

The backbone of SuPreMeChiF is a two-sample Kolmogorov-Smirnov (K-S) test, which statistically evaluates the difference between cumulative distribution functions (CDFs) of two datasets, T(x) and R(x), to determine if they differ significantly (Kolmogorov, 1933; Massey Jr, 1951; Smirnov, 1939). The difference between the datasets is denoted as K-S statistic D and is mathematically represented by Equation [1].

$$D_i = max|T(x_i) - R(x_i)| \quad [1]$$

The two datasets we compare are the scalograms of assigned reference and sample windows. Depending on the window lengths, each window comprises a group of PSDs. We then use a two-sample K-S test to compare, bin by bin, the distribution of the PSDs in the reference window (RW) and in the sample window (SW). The resulting K-S statistic, D, measures the maximum difference between their cumulative distributions. Each bin (indexed with *i*) at each timestamp produces one D, resulting in a D-matrix that will be presented in pseudocolor plot later on. Equation [2] is used to associate D values from *k* number of bins and produces a single change index at each timestamp. It is also possible to look at specific frequency ranges by assigning the starting (*i*) and ending (*k*) index of the bins for calculating the change index.

$$Change\ index = \sqrt{\sum_{i=1}^{k} D_i^2} \qquad [2]$$

The SW and RW are shifted together along the timeline at a given rate. Each move generates a change index that will be assigned to the end of the associated SW. As a result, for a given reference and sample window combination, we produce a time-series of change indexes with resolution depending on the shifting rate. We initially consider the full frequency range, and later focus on more specific ranges catering to events of interest.

Changes or perturbations in a volcanic system may trigger changes in the frequency content of the waveform data and be caught in the SW. As a result, a larger mismatch between their CDFs and therefore a larger K-S statistic D or a peak in the time-series of change indexes is expected. (See Supplement Fig.S1)

2.3 Synthetic results

We first test SuPreMeChiF on a synthetic waveform (Fig.1a and Fig.1b). The six-day synthetic waveform has constant noise at 10Hz. Signals of 5Hz, 0.5Hz and 15Hz, with a length 3 days, are introduced at the start of day 2, day 3, and day 4 respectively. In this test case we use SW and RW of length 1 and 12 hours respectively. SW immediately follows RW, and both windows are shifted along the timeline at a rate of 0.5 hours.

The resulting change index time-series (Fig.1c) indicates a sudden increase when SW enters data with new frequency content. The statistics reach a maximum at the timestamp when SW is completely sampling the new frequency content, while RW is sampling the old frequency content. The change index declines gradually once the RW moves into the same new frequency zone and is at a minimum when both windows sample the same frequency content again. The pseudocolor plot of D-matrix has peaks at the time and frequency when the frequency change occurs (Fig.1d). We calculate the median, 16 and 84 percentiles (one standard deviation from the mean) of the constituent D values to verify data coherence.

We also test the impact of RW and SW window lengths on the D statistic and change index time series. Shorter window lengths produce sharper peaks and therefore clearer detections of change (Fig.1e and 1f). Depending on the event type of interest, the window lengths, particularly the ratio between RW and SW can be optimised - this is further investigated in the later sections using real data.

It is important to note that the change indexes should be referenced to the end of the sample window. This is intuitive because the statistics can only be generated based on past data; meaning a delay of sample-window length should be expected for each detection made. It is also observed that longer window sizes would optimise the detection quality because more data points are used, and the resulting curve is smoother. Therefore, when determining optimal window sizes for the analysis, we have to consider a trade-off between window length and the detection ability. In this paper, all results were aligned with the physical happening of events for a clearer visualisation (i.e., the sample window length is subtracted from the change index time).

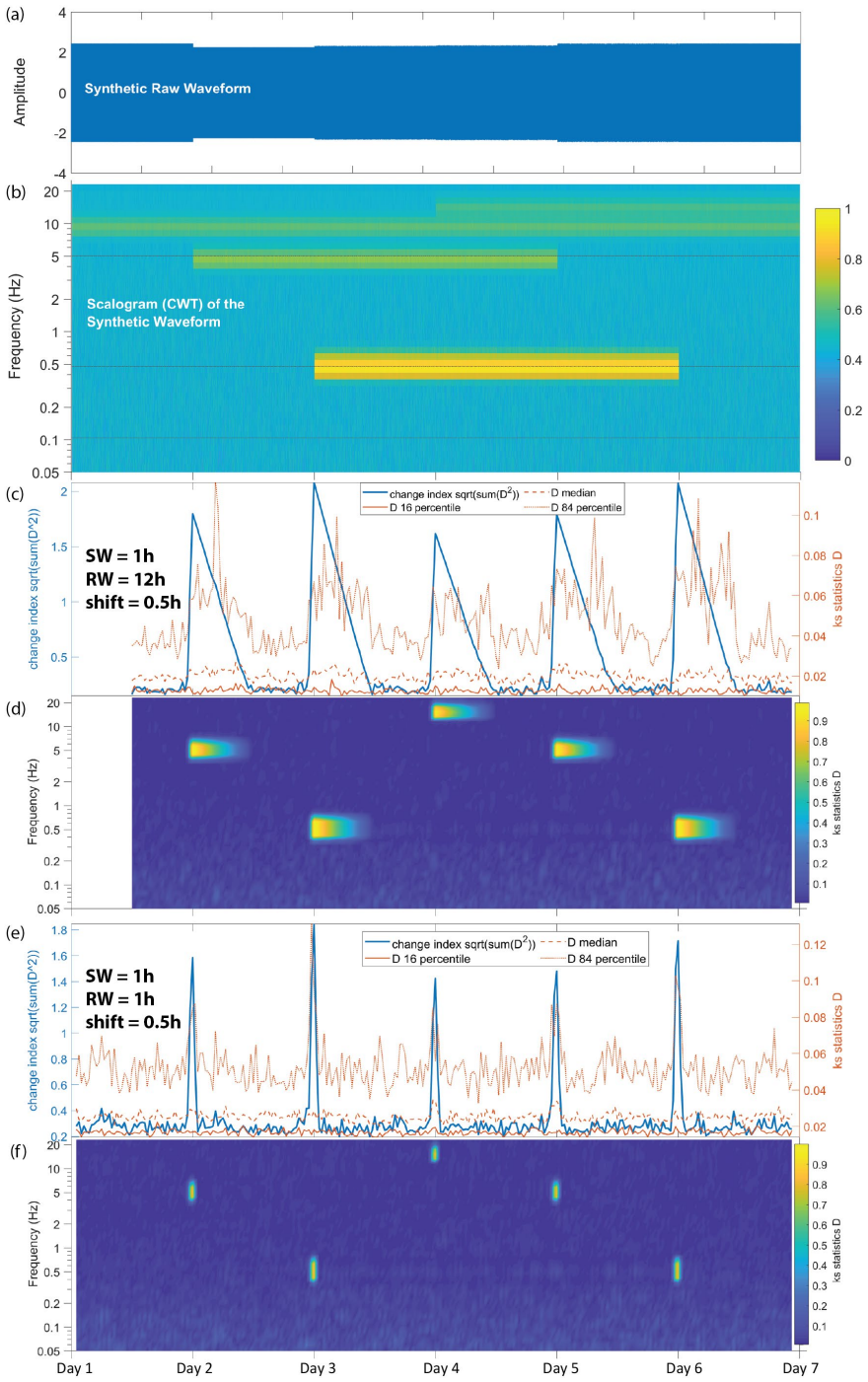

185

186 **Figure 1**. SuPreMeChiF synthetic waveform results, illustrating the impact of RW and SW
187 lengths on detecting spectral changes. **(a)** Synthetic waveform. **(b)** Scalogram. **(c)** Change index
188 time-series and **(d)** D-matrix presented in pseudocolor plot using 1-hour SW, 12-hour RW. **(e)**
189 Change index time-series and **(f)** D-matrix using 1-hour SW and 1-hour RW.

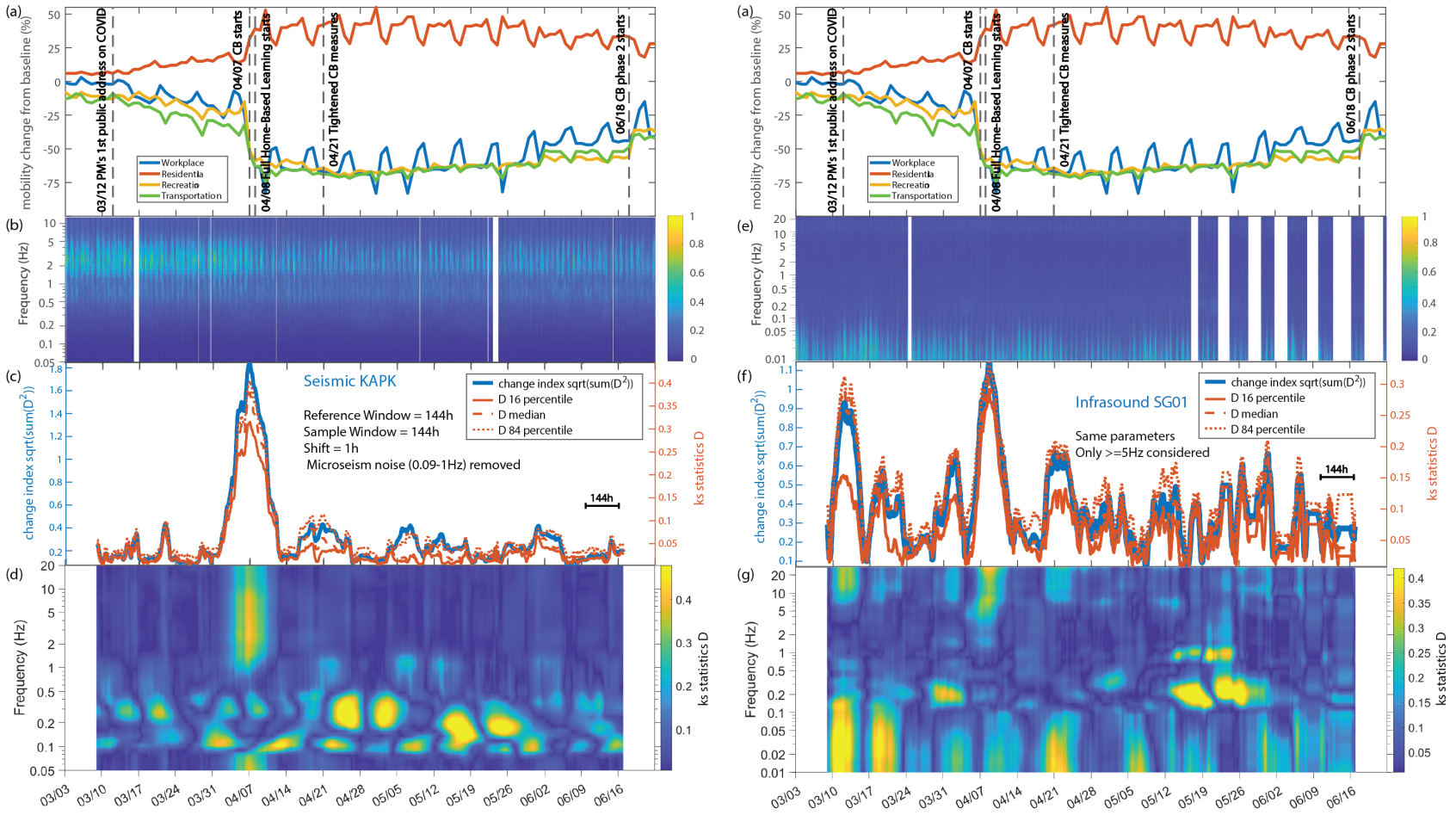

Figure 2. SuPreMeChiF results on seismic (left column) and infrasound (right column) recordings in Singapore during COVID-19 lockdown. **(a)** Singapore's mobility change from baseline from Google mobility report. Key events are marked by dash lines. **(b)** Scalogram, **(c)** change index time-series, **(d)** D-matrix presented in pseudocolor plot for seismic data from KAPK. **(e)** Scalogram, **(f)** change index time-series, **(g)** D-matrix pseudocolor plot for infrasound data from SG01.

195 **3 Case study: COVID-19 lockdown in Singapore**

196 The COVID-19 pandemic in 2020 saw the introduction of widespread restrictions on
197 human activity. This unprecedented reduction in human activities caused a large drop in
198 anthropogenic seismic and acoustic noise. Mean seismic power reductions of up to 50% were
199 observed in some locations (Kuponiyi & Kao, 2021; Lecocq et al., 2020; Roy et al., 2021). The
200 average amplitude of acoustic noise also reduced, with some locations recording a halving of
201 acoustic noise (Bird et al., 2021; Spivak et al., 2021).

202 In Singapore, a nationwide partial lockdown called a Circuit Breaker (CB), was
203 implemented in early 2020. Mobility data shows that movement related to work, transportation
204 and recreation decreased drastically, while residential mobility increased, in response to the
205 lockdown measures (Fig.2a). Given the expected changes in seismic and infrasound noise in
206 urban Singapore during the lockdown, this period provides a unique test for our SuPreMeChiF
207 method.

208 3.1 COVID-19 timeline in Singapore

209 The first confirmed COVID-19 case appeared in Singapore on 23rd Jan 2020, with the
210 number of cases quickly increasing. On 26th March, entertainment venues were closed,
211 and social gatherings were restricted. Full lockdown measures were enforced on 7th
212 April, closing workplaces, schools and dining-in at eateries. Measures were later
213 tightened on 21st April. On 1st June, Singapore exited CB with small-scale visits
214 allowed, although workplaces and schools remained closed. Measures were further
215 relaxed on 19th June.

216 3.2 Singapore data

217 We use locally collected seismic and infrasound monitoring data for a continuous
218 112-day period in 2020. Seismic data are from the KAPK wideband station located in the
219 south-eastern part of Singapore, near to the coast. KAPK hosts a Kinemetrics WR-1
220 wide-band seismometer that has flat response between 0.05-20Hz and samples at 100Hz.
221 Infrasound data are from the SG01 infrasound station located in MacRitchie Reservoir,
222 central Singapore. It has a Seismowave MB2005 microbarometer which has flat response

223 between 0.01-27Hz and samples at 80Hz. Stations KAPK and SG01 are approximately
224 10 kilometres apart (Fig.4a).

225 Fig 2b and 2e shows scalograms for stations KAPK and SG01 during the CB
226 period. There is a visually distinguishable change in spectral properties of the seismic
227 data related to Singapore's lockdown measures, particularly the enforcement of the CB
228 period on 7th April. However, changes in the infrasound scalogram are not as clear,
229 which may indicate that the background is too noisy and/or the change is too small to be
230 seen in the acoustic data. This setting provides us with an opportunity to test the
231 detectability of SuPreMeChiF on subtle changes that cannot be identified on a simple
232 scalogram or spectrogram.

233 3.3 Choice of parameters

234 Seismic and infrasound data in Singapore has a large overprint from diurnal
235 changes in human activity. To minimise the anthropogenic diurnal impact on the result,
236 we test a range of window sizes from 1 to 20 days, with an interval of 24 hours. Results
237 from selected sets of reference and sample windows are presented in Fig.3, including our
238 chosen window size of 144 hours (6 days). The temporal shift is 1 hour, which balances
239 computational cost and detection promptness.

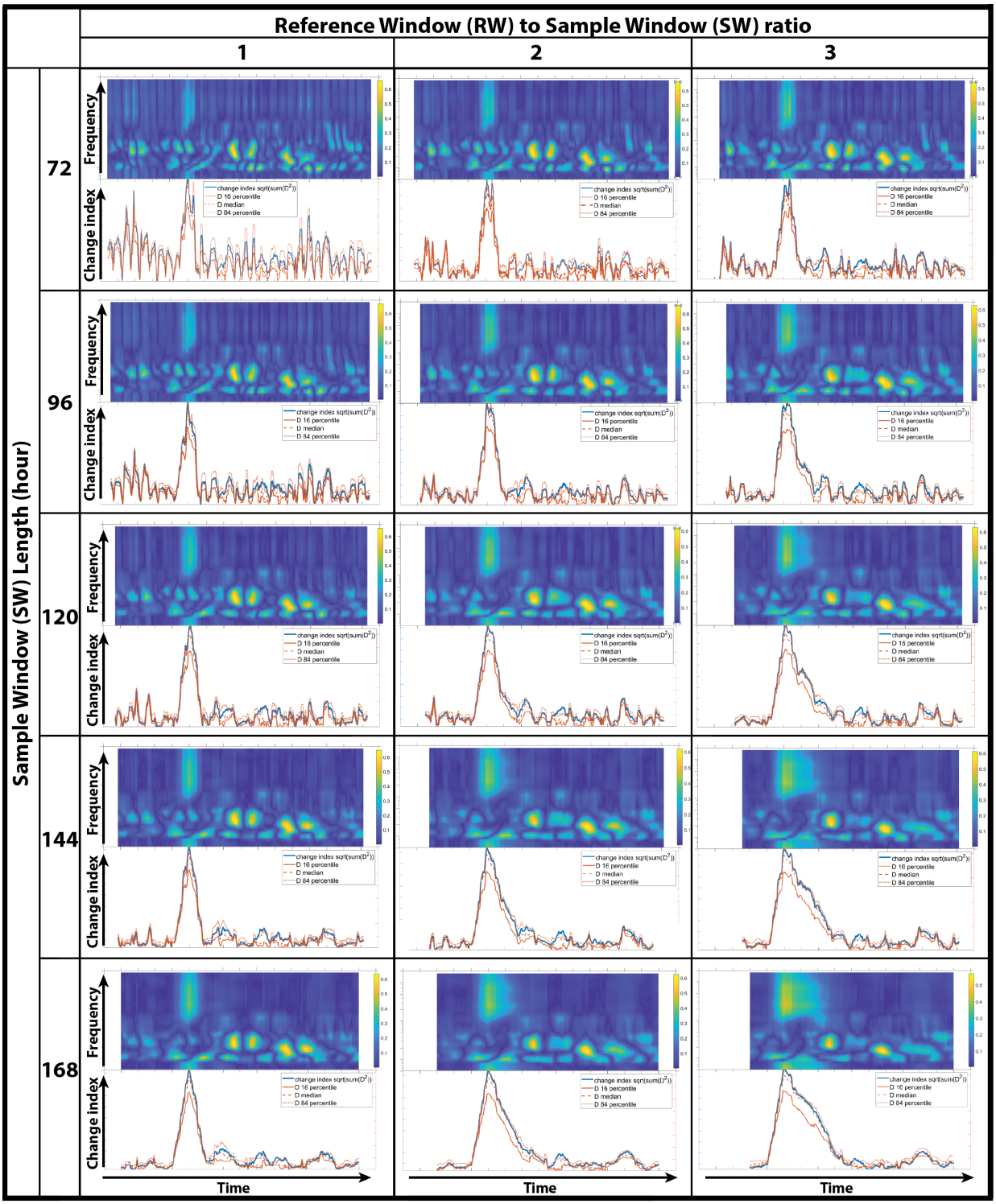

Figure 3. Results for a range of reference and sample window lengths. Upper panel in each cell is the D-matrix plots showing the spectral range where changes took place in. Lower panels are the change index time-series obtained from each D-matrix, excluding D values from microseism range (0.09-1Hz).

4 Identification and interpretation of changes

In Figure 2, we compare the SuPreMeChiF results with the mobility change time-series of Singapore during CB, and find:

- Changes in the human activities were reflected in a certain frequency range - above 1~2Hz in seismic and above 5Hz in infrasound. Natural signals such as microseism and microbarom were also picked up.
- Both the seismic and infrasound change index time-series agree with the CB timeline. Changes observed in the seismic result agree with its scalogram (Fig.2b). Clear detections were also made in the infrasound data which were not clear in its scalogram (Fig.2e).

4.1 Changes reflected in a certain frequency range

We first investigate the intensity and spectral range of changes, by formatting the individual K-S statistics D at each timestamp and frequency bin into a D-matrix, which is then presented in pseudocolor plots (Fig.2d and 2g). The seismic D-matrix shows that changes reflecting CB generally occur at frequencies greater than 1Hz (Fig.2d). On the other hand, changes in infrasound data are largest above 5Hz (Fig.2g).

In both seismic and infrasound D-matrix plots, a band of higher variability is observed at frequencies below approximately 1Hz. Given that Singapore is a small island country bounded by two straits, this low frequency band likely represents the natural microseism and microbarom generated by ocean waves surrounding Singapore. We verify this by analysing two additional local seismic stations (location as shown in Fig.4a). All three seismic stations show comparable detection results that match with the CB timeline, in addition to having a band of persistent change in a similar low frequency range (See Supplement Fig.S2). Two frequency bands are evident: one between 0.2-0.5Hz which is consistent with the frequency range of the secondary microseism (produced by wave-wave interactions), and the other at approximately 0.08-0.15Hz, which is consistent with the primary microseism due to the impact of waves on a sloping seafloor in coastal areas (Ardhuin et al., 2015; Hasselmann, 1963).

272 4.2 Agreement with the CB timeline

273 We associate a group of K-S statistic Ds at each timestamp, to form change index
274 time-series of certain frequency range. We exclude the microseism range (0.09-1Hz) for
275 seismic and non-anthropogenic range (<5Hz) for infrasound. SuPreMeChiF results show
276 that changes that were not clear in raw scalograms (Fig.2b and 2e) became
277 distinguishable, indicated by a peak in each figure (Fig.2c and 2f). The exact time and
278 extent of the increase in the statistics could be easily retrieved and compared across the
279 timeline; therefore, the onset time and the amount of change can be quantified.

280 By aligning with the mobility change and CB timeline (Fig.2a), the seismic
281 change index peak begins ~six days before and ends ~six days after the centre of the
282 peak, which occurs precisely at the onset date of CB (Fig. 2c). The 6-day timeframe can
283 be explained by the length of sample and reference window used. The increase in change
284 index started when the sample window entered the post-CB phase, reached the maximum
285 when the sample window was fully post-CB and the reference window fully pre-CB, and
286 ended when both windows reached the post-CB phase. Mobility data indicates there is a
287 gradual return to pre-CB level over the following two months, and no substantial increase
288 in the seismic change index is recorded.

289 Infrasound results have a peak one day later than the seismic data, on 8th April
290 2020. This is one day after the onset of CB, (Fig.2d) and corresponds to the start of
291 school closures in Singapore. The slight time difference between infrasound and seismic
292 changes suggests that the signals could respond differently to various types of activities.

293 More variations are observed in the infrasound results, compared to seismic.
294 Seismic monitoring in a city setting is highly subjective to proximal vibrational sources.
295 On the other hand, infrasound with its long wavelength, attenuates less while travelling
296 and covers a wider region. Therefore, it may have better detection performance for the
297 general changes islandwide. For example, (Fig.2c), the first peak in the infrasound results
298 on 12th March may be associated with the general mobility decrease after the first Prime
299 Minister's (PM) public address on COVID-19. According to the local news, there was a
300 surge in grocery shopping across the country. The peak on 22nd April may indicate some

behavioural change in the community due to the tightened CB measures announced by the PM the day before.

5 Application to volcano monitoring

We have verified the performance of SuPreMeChiF to detect subtle changes in continuous data, using both synthetic, seismic and infrasound data in urban settings. The same approach could be applied to other environments such as volcanoes.

The D-matrix plots (Fig.2d and 2g) provide information on the spectral ranges at which the changes occur. By combining volcano physics and D-matrix observations, we could visually capture the extent of any change and potentially identify the corresponding source. For instance, SuPreMeChiF has potential for the detection of phreatic eruptions, which many studies have claimed to have no or few precursors (Barberi et al., 1992; JMA, 2014). However post-eruption analysis has identified the emergence of very-long-period (VLP) events months to seconds prior to phreatic explosions (Jolly et al., 2017; Kaneshima et al., 1996; Kawakatsu et al., 2000; Maeda et al., 2015a; Ohminato, 2006). VLP events, with a period of 2-100s, signify a pressurised hydrothermal system. SuPreMeChiF has potential to identify VLP events in their characteristic spectral range, opening a possibility to forecast phreatic eruptions.

VLP activity could share the same spectral range as ocean-generated microseisms (~<1 Hz), however, SuPreMeChiF's adaptable parameterisation allows separation of signals in the same frequency range by varying window lengths to the events of interest. For example, using long reference and sample windows, allows the detection of a long-term change in human mobility trend (Fig.2). On the other hand, a short sample window (30 minutes) and relatively-long reference window (24 hours) acts like a short-term event detector and allows detection of remote tectonic events (Fig.4b and 4c). Similarly, the reference and sample window lengths can be tuned for VLP event detection, particularly by using shorter window lengths.

Since infrasound has low attenuation, it travels long distances with minimal energy loss. Therefore, SuPreMeChiF applied to volcanogenic infrasound would be an effective way of detecting a remote volcanic eruption. The change index time-series make it easier to set an automated alert threshold and flag detection when the threshold is passed.

As a real-time detector for precursory activities in a volcanic system, timeliness is a key factor. The current real-time detection would have a lag period of a sample window length. Therefore, a careful choice of window length is important, and parameters should be optimised for different settings.

A further limitation is that, similar to other techniques, the performance of SuPreMeChiF largely relies on the location of the monitoring instrument, i.e., proximity to the source. Detection coherence across multiple stations would boost confidence in the detection and acts as an additional indicator to flag an event.

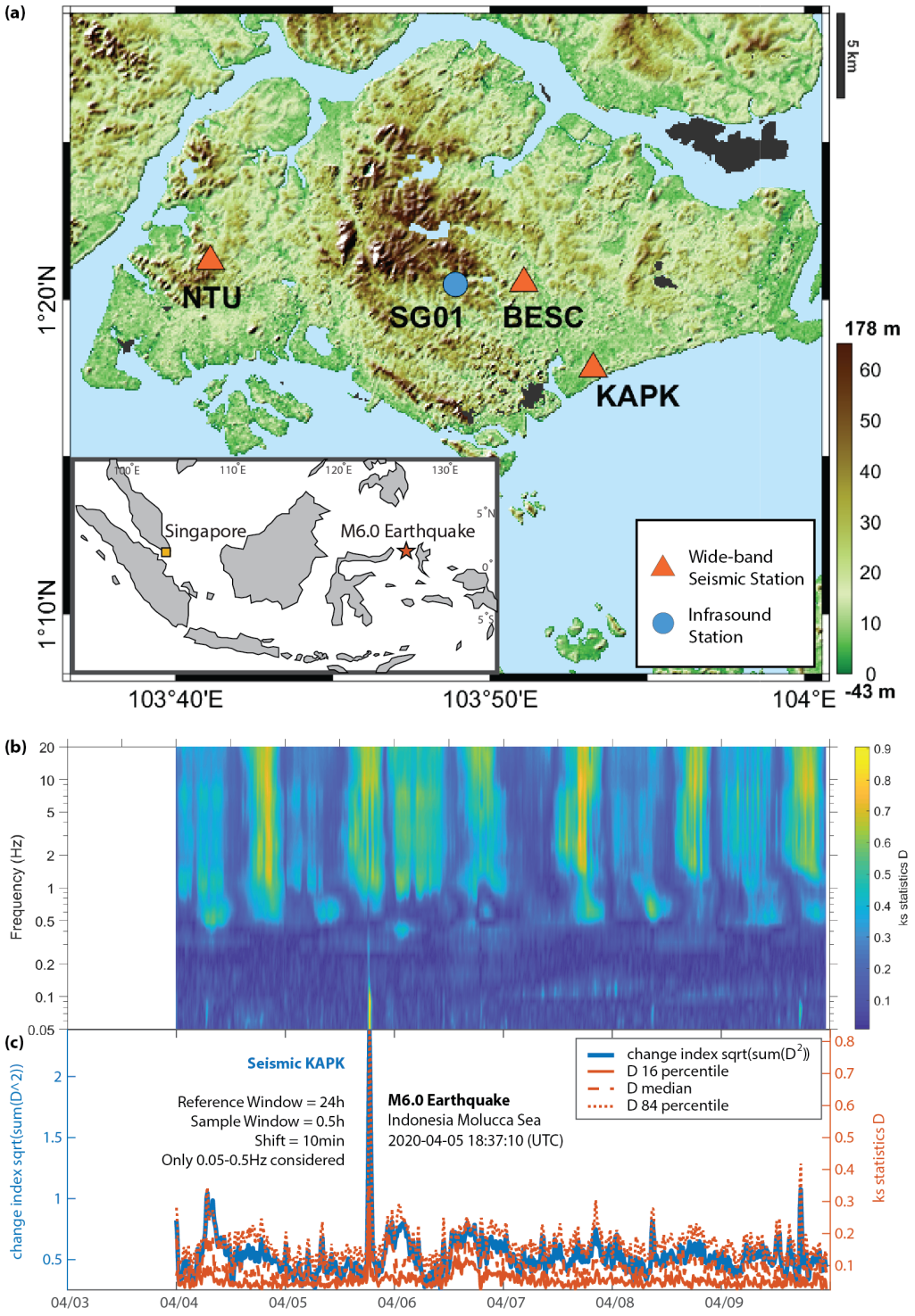

Figure 4. (a) Singapore map indicating seismic and infrasound stations used. Inset shows location of Singapore and the M6.0 earthquake. **(b)** D-matrix and **(c)** change index for 0.05-0.5Hz.

6 Conclusions

We introduce a new technique — Subtle Precursory Meaningful Changes in Frequency (SuPreMeChiF), to statistically detect subtle changes in a system. The highlight of the method is the ability to quantify the amount of deviation in monitoring data, including subtle changes that may be overlooked using conventional analysis. SuPreMeChiF also shows the spectral range where changes took place and therefore has potential to indicate the source of change. Our case study on seismic and infrasound recordings during the COVID period in Singapore shows alignment between SuPreMeChiF results and the lockdown timeline, demonstrating the effectiveness in detecting background noise variations due to human mobility change. The method could be applied on natural systems, such as volcano monitoring data. This presents the opportunity to re-assess past un-forecasted eruptions, aiming to detect subtle precursory changes that may have been overlooked or missed by previous analysis, in a systematic and quantitative way. The method could also be used to assess whether the system has returned to pre-perturbed status by using a fixed reference window characteristic of the non-perturbed state and a moving sample window along the timeline. Further work could also include multiparametric monitoring data. With some adjustment on the detection parameters based on settings, the detections for precursory activities can be automated in near real-time.

Acknowledgments

We acknowledge the Meteorological Services of Singapore for operating the seismic stations under the International Federation of Digital Seismograph Network (FDSN). We would also like to acknowledge Earth Observatory of Singapore (EOS) Team Magma Infrasound Group and EOS Centre for Geohazard Observations (CGO) for establishing and maintaining the Singapore infrasound network. I would also like to express my great gratitude to Prof. Jürgen Neuberg for constructive advice on improving the SuPreMeChiF method along the way. This research was supported by the Earth Observatory of Singapore (grant number 04MNS001807A620OOE01 - Lab Volcanoes) via its funding from the National Research Foundation Singapore and the Singapore Ministry of Education under the Research Centres of Excellence initiative. This work comprises EOS contribution number 497.

Open Research

All seismic data and related metadata used in this paper are stored in IRIS Data Management Center (IRIS-DMC) and accessible via Federation of Digital Seismograph Networks (FDSN) services under network identifier MS, which may be found at https://www.fdsn.org/networks/detail/MS/. All infrasound data used in this paper are available at Nanyang Technological University research data repository DR-NTU (Data) via https://doi.org/10.21979/N9/1ZRELD. The Singapore mobility data were retrieved from Google COVID-19 Community Mobility Report provided by Google LLC (https://www.google.com/covid19/mobility/). We use MATLAB R2018b and its Signal Processing Toolbox™ for all the analysis, including fetching data from IRIS, the SuPreMeChiF analysis, the generation of figures and maps (MATLAB, 2018).

References

Aki, K., & Koyanagi, R. (1981). Deep volcanic tremor and magma ascent mechanism under Kilauea, Hawaii. Journal of Geophysical Research: Solid Earth, 86(B8), 7095-7109. https://doi.org/10.1029/JB086iB08p07095

Ardhuin, F., Gualtieri, L., & Stutzmann, E. (2015). How ocean waves rock the Earth: Two mechanisms explain microseisms with periods 3 to 300 s. Geophysical Research Letters, 42(3), 765-772. https://doi.org/10.1002/2014GL062782

Barberi, F., Bertagnini, A., Landi, P., & Principe, C. (1992). A review on phreatic eruptions and their precursors. Journal of Volcanology and Geothermal Research, 52(4), 231-246. https://doi.org/10.1016/0377-0273(92)90046-G

Bebbington, M. S. (2013). Assessing probabilistic forecasts of volcanic eruption onsets. Bulletin of Volcanology, 75(12), 783. https://doi.org/10.1007/s00445-013-0783-5

Bird, E. J., Bowman, D. C., Seastrand, D. R., Wright, M. A., Lees, J. M., & Dugick, F. K. D. (2021). Monitoring changes in human activity during the COVID-19 shutdown in Las Vegas using infrasound microbarometers. The Journal of the Acoustical Society of America, 149(3), 1796-1802. https://doi.org/10.1121/10.0003777

Brenguier, F., Shapiro, N. M., Campillo, M., Ferrazzini, V., Duputel, Z., Coutant, O., & Nercessian, A. (2008). Towards forecasting volcanic eruptions using seismic noise. Nature Geoscience, 1(2), 126-130. https://doi.org/10.1038/ngeo104

Burt, M. L., Wadge, G., & Scott, W. A. (1994). Simple stochastic modelling of the eruption history of a basaltic volcano: Nyamuragira, Zaire. Bulletin of Volcanology, 56(2), 87-97. https://doi.org/10.1007/BF00304104

Carniel, R., Jolly, A. D., & Barbui, L. (2013). Analysis of phreatic events at Ruapehu volcano, New Zealand using a new SOM approach. Journal of Volcanology and Geothermal Research, 254, 69. https://doi.org/10.1016/j.jvolgeores.2012.12.026

Caudron, C., Taisne, B., Neuberg, J., Jolly, A. D., Christenson, B., Lecocq, T., Suparjan, Syahbana, D., & Suantika, G. (2018). Anatomy of phreatic eruptions. Earth, Planets and Space, 70(1), 168. https://doi.org/10.1186/s40623-018-0938-x

409 Chakraborty, A., & Okaya, D. (1995). Frequency-time decomposition of seismic data using wavelet-
410 based methods. Geophysics, 60(6), 1906-1916. https://doi.org/10.1190/1.1443922

411 Chouet, B. A., & Matoza, R. S. (2013). A multi-decadal view of seismic methods for detecting precursors
412 of magma movement and eruption. Journal of Volcanology and Geothermal Research, 252, 108-175.
413 https://doi.org/10.1016/j.jvolgeores.2012.11.013

414 Cong, F., Chen, J., & Pan, Y. (2011). Kolmogorov-Smirnov test for rolling bearing performance
415 degradation assessment and prognosis. Journal of vibration and control, 17(9), 1337-1347.
416 https://doi.org/10.1177/1077546310384003

417 Doherty, A. L. (2009). Blue-sky eruptions, do they exist?: implications for monitoring New Zealand's
418 volcanoes. http://dx.doi.org/10.26021/7865

419 Endo, E. T., & Murray, T. (1991). Real-time seismic amplitude measurement (RSAM): a volcano
420 monitoring and prediction tool. Bulletin of Volcanology, 53(7), 533-545.
421 https://doi.org/10.1007/BF00298154

422 Germanovich, L. N., & Lowell, R. P. (1995). The mechanism of phreatic eruptions. Journal of
423 Geophysical Research: Solid Earth, 100(B5), 8417-8434. https://doi.org/10.1029/94JB03096

424 Gudmundsson, M. T., Thordarson, T., Höskuldsson, Á., Larsen, G., Björnsson, H., Prata, F. J., Oddsson,
425 B., Magnússon, E., Högnadóttir, T., Petersen, G. N., Hayward, C. L., Stevenson, J. A., & Jónsdóttir, I.
426 (2012). Ash generation and distribution from the April-May 2010 eruption of Eyjafjallajökull, Iceland.
427 Scientific Reports, 2(1), 572. https://doi.org/10.1038/srep00572

428 Hansen, J., Lacis, A., Ruedy, R., & Sato, M. (1992). Potential climate impact of Mount Pinatubo eruption.
429 Geophysical Research Letters, 19(2), 215-218. https://doi.org/10.1029/91GL02788

430 Hasselmann, K. (1963). A statistical analysis of the generation of microseisms. Reviews of Geophysics,
431 1(2), 177-210. https://doi.org/10.1029/RG001i002p00177

432 Janda, R. J., Daag, A. S., Newhall, C. G., Pierson, T. C., Punongbayan, R. S., Rodolfo, K. S., Solidum, R.
433 U., & Umbal, J. V. (1996). Assessment and response to lahar hazard around Mount Pinatubo, 1991 to
434 1993. In R. P. C.G. Newhall (Ed.), Fire and Mud: Eruptions and Lahars of Mount Pinatubo, Philippines
435 (pp. 107-139). Quezon City: Philippine Institute of Volcanology and Seismology.

JMA. (2014). Ontakesan (September 2014 Issue). Monthly commentary documents on volcanic activity. Retrieved from http://www.data.jma.go.jp/svd/vois/data/tokyo/STOCK/monthly_v-act_doc/tokyo/14m09/312_14m09.pdf

Jolly, A. D., Lokmer, I., Christenson, B., & Thun, J. (2018). Relating gas ascent to eruption triggering for the April 27, 2016, White Island (Whakaari), New Zealand eruption sequence. Earth, Planets and Space, 70(1), 177. https://doi.org/10.1186/s40623-018-0948-8

Jolly, A. D., Lokmer, I., Thun, J., Salichon, J., Fry, B., & Chardot, L. (2017). Insights into fluid transport mechanisms at White Island from analysis of coupled very long-period (VLP), long-period (LP) and high-frequency (HF) earthquakes. Journal of Volcanology and Geothermal Research, 343, 75-94. https://doi.org/10.1016/j.jvolgeores.2017.06.006

Jolly, G., Sandri, L., Lindsay, J., Scott, B., Sherburn, S., Jolly, A., Fournier, N., Keys, H., & Marzocchi, W. (2010). Volcanic risk metrics at Mt Ruapehu, New Zealand: some background to a probabilistic eruption forecasting scheme and a cost/benefit analysis at an open conduit volcano. Paper presented at the EGU General Assembly Conference Abstracts. https://ui.adsabs.harvard.edu/abs/2010EGUGA..12.2994J

Kaneshima, S., Kawakatsu, H., Matsubayashi, H., Sudo, Y., Tsutsui, T., Ohminato, T., Ito, H., Uhira, K., Yamasato, H., Oikawa, J., Takeo, M., & Iidaka, T. (1996). Mechanism of phreatic eruptions at Aso volcano inferred from near-field broadband seismic obserbvations. Science, 273(5275), 642. https://doi.org/10.1126/science.273.5275.642

Kar, C., & Mohanty, A. (2004). Application of KS test in ball bearing fault diagnosis. Journal of sound and vibration, 269(1-2), 439-454. https://doi.org/10.1016/S0022-460X(03)00380-8

Kawakatsu, H., Kaneshima, S., Matsubayashi, H., Ohminato, T., Sudo, Y., Tsutsui, T., Uhira, K., Yamasato, H., Ito, H., & Legrand, D. (2000). Aso94: Aso seismic observation with broadband instruments. Journal of Volcanology and Geothermal Research, 101(1), 129-154. https://doi.org/10.1016/S0377-0273(00)00166-9

Klose, C. (2006). Self-organizing maps for geoscientific data analysis: geological interpretation of multidimensional geophysical data. Computational Geosciences, 10(3), 265-277. https://doi.org/10.1007/s10596-006-9022-x

Kolmogorov, A. (1933). Sulla determinazione empirica di una lgge di distribuzione. Inst. Ital. Attuari, Giorn., 4, 83-91.

Kuponiyi, A. P., & Kao, H. (2021). Temporal Variation in Cultural Seismic Noise and Noise Correlation Functions during COVID-19 Lockdown in Canada. Seismological Research Letters, 92(5), 3024-3034. https://doi.org/10.1785/0220200330

Langer, H., Falsaperla, S., Masotti, M., Campanini, R., Spampinato, S., & Messina, A. (2009). Synopsis of supervised and unsupervised pattern classification techniques applied to volcanic tremor data at Mt Etna, Italy. Geophysical Journal International, 178(2), 1132-1144. https://doi.org/10.1111/j.1365-246X.2009.04179.x

Lapins, S., Roman, D. C., Rougier, J., De Angelis, S., Cashman, K. V., & Kendall, J. M. (2020). An examination of the continuous wavelet transform for volcano-seismic spectral analysis. Journal of Volcanology and Geothermal Research, 389, 106728. https://doi.org/10.1016/j.jvolgeores.2019.106728

Lecocq, T., Caudron, C., & Brenguier, F. (2014). MSNoise, a Python Package for Monitoring Seismic Velocity Changes Using Ambient Seismic Noise. Seismological Research Letters, 85(3), 715-726. https://doi.org/10.1785/0220130073

Lecocq, T., Hicks, S. P., Van Noten, K., van Wijk, K., Koelemeijer, P., De Plaen, R. S. M., Massin, F., Hillers, G., Anthony, R. E., Apoloner, M.-T., Arroyo-Solórzano, M., Assink, J. D., Büyükakpınar, P., Cannata, A., Cannavo, F., Carrasco, S., Caudron, C., Chaves, E. J., Cornwell, D. G., Craig, D., den Ouden, O. F. C., Diaz, J., Donner, S., Evangelidis, C. P., Evers, L., Fauville, B., Fernandez, G. A., Giannopoulos, D., Gibbons, S. J., Girona, T., Grecu, B., Grunberg, M., Hetényi, G., Horleston, A., Inza, A., Irving, J. C. E., Jamalreyhani, M., Kafka, A., Koymans, M. R., Labedz, C. R., Larose, E., Lindsey, N. J., McKinnon, M., Megies, T., Miller, M. S., Minarik, W., Moresi, L., Márquez-Ramírez, V. H., Möllhoff, M., Nesbitt, I. M., Niyogi, S., Ojeda, J., Oth, A., Proud, S., Pulli, J., Retailleau, L., Rintamäki, A. E., Satriano, C., Savage, M. K., Shani-Kadmiel, S., Sleeman, R., Sokos, E., Stammler, K., Stott, A. E., Subedi, S., Sørensen, M. B., Taira, T. a., Tapia, M., Turhan, F., van der Pluijm, B., Vanstone, M., Vergne, J., Vuorinen, T. A. T., Warren, T., Wassermann, J., & Xiao, H. (2020). Global quieting of high-frequency seismic noise due to COVID-19 pandemic lockdown measures. Science, 369(6509), 1338-1343. https://doi.org/doi:10.1126/science.abd2438

Maeda, Y., Kato, A., Terakawa, T., Yamanaka, Y., Horikawa, S., Matsuhiro, K., & Okuda, T. (2015a). Source mechanism of a VLP event immediately before the 2014 eruption of Mt. Ontake, Japan. Earth, Planets and Space, 67(1), 1-7. https://doi.org/10.1186/s40623-015-0358-0

494 Maeda, Y., Kumagai, H., Lacson Jr., R., Figueroa II, M. S., Yamashina, T., Ohkura, T., & Baloloy, A. V.
495 (2015b). A phreatic explosion model inferred from a very long period seismic event at Mayon Volcano,
496 Philippines. Journal of Geophysical Research: Solid Earth, 120(1), 226-242.
497 https://doi.org/10.1002/2014jb011440

498 Marchetti, E., van Herwijnen, A., Christen, M., Silengo, M. C., & Barfucci, G. (2020). Seismo-acoustic
499 energy partitioning of a powder snow avalanche. Earth Surf. Dynam., 8(2), 399-411.
500 https://doi.org/10.5194/esurf-8-399-2020

501 Massey Jr, F. J. (1951). The Kolmogorov-Smirnov test for goodness of fit. Journal of the American
502 statistical Association, 46(253), 68-78.

503 MATLAB. (2018). version 9.5.0.1033004 (R2018b). Natick, Massachusetts: The MathWorks Inc.

504 Matthews, A. J., Barclay, J., Carn, S., Thompson, G., Alexander, J., Herd, R., & Williams, C. (2002).
505 Rainfall-induced volcanic activity on Montserrat. Geophysical Research Letters, 29(13), 22-21-22-24.
506 https://doi.org/10.1029/2002GL014863

507 Mulargia, F., Gasperini, P., & Tinti, S. (1987). Identifying different regimes in eruptive activity: An
508 application to Etna volcano. Journal of Volcanology and Geothermal Research, 34(1), 89-106.
509 https://doi.org/10.1016/0377-0273(87)90095-3

510 Neuberg, J. (2000). External modulation of volcanic activity. Geophysical Journal International, 142(1),
511 232-240. https://doi.org/10.1046/j.1365-246x.2000.00161.x

512 Ohminato, T. (2006). Characteristics and source modeling of broadband seismic signals associated with
513 the hydrothermal system at Satsuma–Iwojima volcano, Japan. Journal of Volcanology and Geothermal
514 Research, 158(3), 467-490. https://doi.org/10.1016/j.jvolgeores.2006.08.004

515 Roy, K. S., Sharma, J., Kumar, S., & Kumar, M. R. (2021). Effect of coronavirus lockdowns on the
516 ambient seismic noise levels in Gujarat, northwest India. Scientific Reports, 11(1), 7148.
517 https://doi.org/10.1038/s41598-021-86557-9

518 Seropian, G., Kennedy, B. M., Walter, T. R., Ichihara, M., & Jolly, A. D. (2021). A review framework of
519 how earthquakes trigger volcanic eruptions. Nature Communications, 12(1), 1004.
520 https://doi.org/10.1038/s41467-021-21166-8

Smirnov, N. V. (1939). On the estimation of the discrepancy between empirical curves of distribution for two independent samples. Bull. Math. Univ. Moscou, 2(2), 3-14.

Smittarello, D., Smets, B., Barrière, J., Michellier, C., Oth, A., Shreve, T., Grandin, R., Theys, N., Brenot, H., Cayol, V., Allard, P., Caudron, C., Chevrel, O., Darchambeau, F., de Buyl, P., Delhaye, L., Derauw, D., Ganci, G., Geirsson, H., Kamate Kaleghetso, E., Kambale Makundi, J., Kambale Nguomoja, I., Kasereka Mahinda, C., Kervyn, M., Kimanuka Ruriho, C., Le Mével, H., Molendijk, S., Namur, O., Poppe, S., Schmid, M., Subira, J., Wauthier, C., Yalire, M., d'Oreye, N., Kervyn, F., & Syavulisembo Muhindo, A. (2022). Precursor-free eruption triggered by edifice rupture at Nyiragongo volcano. Nature, 609(7925), 83-88. https://doi.org/10.1038/s41586-022-05047-8

Sparks, R. S. J. (2003). Forecasting volcanic eruptions. Earth and Planetary Science Letters, 210(1), 1-15. https://doi.org/10.1016/S0012-821X(03)00124-9

Spivak, A. A., Loktev, D. N., Rybnov, Y. S., & Kharlamov, V. A. (2021). Acoustic Noise in Moscow during the Covid-19 Quarantine Period in 2020. Doklady Earth Sciences, 496(1), 63-65. https://doi.org/10.1134/S1028334X21010232

Wang, X., & Makis, V. (2009). Autoregressive model-based gear shaft fault diagnosis using the Kolmogorov–Smirnov test. Journal of sound and vibration, 327(3-5), 413-423. https://doi.org/10.1016/j.jsv.2009.07.004